J. Pestic. Sci. **45**(3), 166–176 (2020)
DOI: 10.1584/jpestics.J20-01

Sociality Awards 2020
(on prominent achievement)

Theoretical and organic chemical approaches to environmental behavior and metabolism of pesticides

Toshiyuki Katagi

Bioscience Research Laboratory, Sumitomo Chemical Co., Ltd., 3–1–98 Kasugadenaka, Konohana-ku, Osaka 554–8558, Japan

(Accepted April 9, 2020)

Investigation of the dissipation and transformation of pesticide through laboratory experiments, conducted in accordance with standard and newly developed designs, gives us valuable information to understand their environmental behavior. We have also been investigating the mechanisms of partition and transformation reactions of pesticides, not only through kinetic analyses, but also through theoretical approaches based on their molecular properties estimated using various spectroscopies and molecular orbital calculations. Furthermore, synthetic iron porphyrin with a peroxide was shown to be a good model to simulate the P450-catalyzed oxidation in the metabolism of pesticides. Through these investigations, the knowledge of surface water, soil, sediment, and plants, such as their properties and constituents, was found indispensable to a deep understanding of the mechanism in the hydrolysis, photolysis, and metabolism of pesticides.

Keywords: environmental behavior of pesticide, spectroscopy, kinetic analysis, theoretical approach, reaction mechanism.

Introduction

Environmental risk assessment of a pesticide is basically conducted by comparing its potential toxicity in nontarget species with its predicted environmental concentration (PEC). The former information is generally collected through many acute and chronic toxicity studies, which are conducted according to the standardized test guidelines, such as those prescribed by the OECD and US EPA. The PEC in an individual compartment, such as water and soil, can be estimated by using the pesticide profiles of partition and degradation therein, whose information is similarly collected from the corresponding standardized studies. First, it should be noted that the experimental conditions in each study are designed by simplifying the typical environment. For example, hydrolysis is generally conducted in a sterile dilute buffer at pH 5–9 and 25°C, while natural water, with the temperature varying diurnally, contains various kinds of suspended matters and dissolved organic compounds, which can be associated with a pesticide molecule depending on its hydrophobicity.[1] Furthermore, many kinds of microbes inhabit natural water, but their effects on pesticide transformations are excluded by sterilization.[2] An aerobic soil metabolism study using regional soil is conducted under a constant water content and temperature, both of which generally fluctuate in the field.[3] A water-sediment study examines multiple processes, such as partition, hydrolysis and microbial metabolism, at the same time, but either the dark condition or the absence of algae/aquatic plants may lead to pesticide behavior different from that in the aquatic environment.[4,5] Additionally, the standard studies examining physicochemical properties and environmental fate are conducted for an active ingredient, and so the effect of formulation on the pesticide behavior cannot be examined.[6] Second, multiple reactions proceed simultaneously in the environment, in contrast to many standardized studies. The aerobic or anaerobic transformation of a pesticide by soil microbes is examined *via* metabolism studies, but the chemical reactions caused by the soil constituents, such as clay minerals,[7] cannot be distinguished unless the soil is appropriately sterilized. A plant metabolism study of a pesticide is usually conducted in a greenhouse or a permitted field, and its photolysis proceeds at the same time on a plant surface.[7,8]

Since the simple interpretation of individual laboratory data may result in estimating an unrealistic environmental concentration of pesticide, in addition to field residue studies, many kinds of computer simulations considering the above environmental factors have been developed and utilized to predict a pesticide's PEC as accurately as possible to that in the environ-

To whom correspondence should be addressed.
E-mail: katagi@sc.sumitomo-chem.co.jp
Published online June 24, 2020

BY-NC-ND © Pesticide Science Society of Japan 2020. This is an open access article distributed under the Creative Commons Attribution-NonCommercial-NoDerivatives 4.0 International (CC BY-NC-ND 4.0) License (https://creativecommons.org/licenses/by-nc-nd/4.0/)

ment. Knowing not only the transformation rate of the pesticide but also its reaction mechanism is indispensable to effectively conduct any simulation. The reaction mechanism can be partly speculated from both the chemical structure of the pesticide and the time-dependent distribution of each identified product in the standardized studies, based on the knowledge of organic chemistry and metabolism. However, additional nonstandard studies using a pesticide and/or degradate together with kinetic, spectroscopic, and/or theoretical approaches should be required to clarify a reaction mechanism. From these points of view, we have scrutinized the reaction mechanisms in the environmental fate of our newly developed and existing pesticides, and sometimes examined the usefulness and applicability of newly designed experimental systems, for the purpose of better environmental assessment of pesticides.

1. Partition Phenomena

The distribution of a pesticide in the environment, governed by diffusion and partition, is conveniently described by the partition coefficient of the pesticide between *n*-octanol and water (log K_{ow}). The good correlation of log K_{ow} with both water solubility and soil adsorption coefficient is well known. The log K_{ow} value of a pesticide is also useful to estimate its bioconcentration factor (BCF) in fish,[9] but less correlation was reported in mollusks, algae, crustacean, and insects, probably due to the different physiologies even within each species.[9,10] Furthermore, either the BCF in frogs[11] or acute toxicity in earthworms[12] is well correlated with the log K_{ow} for pesticides and industrial chemicals. Therefore, the experimental methods to measure log K_{ow} have been standardized by the OECD (shake-flask, OECD 107; slow-stirring, OECD 123; HPLC, OECD 117), and among many theoretical estimation methods of log K_{ow}, the fragment constant approach represented by ClogP[13] has succeeded in estimating the value with reliable precision.

1.1. Theoretical estimation of log K_{ow}

The log K_{ow} values of some organophosphorus pesticides (OPs) cannot be estimated by ClogP due to the lack of appropriate fragment parameters. For sixty-seven OP molecules in either the gas or hydrated phase, we have obtained several molecular properties using MNDO-PM3 molecular orbital (MO) calculations to theoretically estimate their log K_{ow}.[14] The new *NW* parameter was conveniently introduced for each functional group to describe its hydrogen-bonding capacity. *NW* was defined as the total number of sites participating as hydrogen donors or acceptors, based on the Wolfenden's concept.[15] Furthermore, by assuming that the free energy of a molecule in *n*-octanol is equal to that in the gas phase, the change of free energy (E_{ow}) through the partition of the OP from *n*-octanol to water was conveniently estimated by PM3–SM3 MO calculations considering the effect of hydration. Among E_{ow} and several electronic parameters, the single correlation of log K_{ow} with E_{LUMO}, the energy level of the lowest unoccupied MO (LUMO), was only satisfactory, implying that the LUMO localized at the (thio)phosphoryl moiety of OP likely interacts with the MOs of a solvent molecule. In contrast, the *NW*, molecular volume (*V*) and surface (*S*) exhibited a higher correlation ($r>0.8$; $V>S$), but the correlation with *V* and *S* was not improved by considering hydration. These results indicated the importance of the van der Waals force and hydrogen bonding to theoretically describe log K_{ow}. The multiple regression analysis gave the following equation for sixty-seven OPs with the highest correlation ($r=0.977$): $\log K_{ow}=0.0314\,V-0.560\,NW-0.418\,E_{LUMO}-1.38$. The unsigned error of our method was satisfactory (0.33 ± 0.25, $n=67$) and close to that of ClogP (0.21 ± 0.24, $n=65$).

1.2. Pesticide Interactions with biota and lipid bilayers

Insecticides are generally deposited on the body surface of insects covered with cuticular waxes which consist of hydrophobic long-chain hydrocarbons, alcohols, aldehydes, acids, and esters.[6,7,16] The pesticide penetration finally to target sites is primarily controlled by its partition to the wax which would be described by log K_{ow}. We have examined the penetration of eleven radio-labeled (^{14}C, ^{3}H) pesticides, including six OPs and five insecticides having a variety of structures, through their topical application to the fifth instar larvae of the common cutworm (*Spodoptera litura*).[17] The rate constant of penetration (k_p) was conveniently examined *via* radioassay of the surface wash fraction with toluene. The log k_p values of six OPs having analogous chemical structures were described by log K_{ow} with a high correlation ($r=-0.97$), supporting the importance of the partition process governed by pesticide hydrophobicity. In contrast, much poor correlation was observed when other pesticides were included, indicating the presence of another controlling factor. Since the insect cuticle consists of chitin, polymer of *N*-acetylglucosamine in a β (1–4) linkage,[16] the penetration of a molecule would be additionally controlled by interactions with this polymer *via* hydrogen bonding. The introduction of the *NW* parameter[14] actually improved the correlation in the multiple regression as follows: $\log k_p=-0.317\log K_{ow}-0.251\,NW+1.47$ ($r=0.94$, $n=11$).

Next, the interaction of the pesticide with biological membranes was investigated using the multilamellar lipid bilayer vesicle (MLV) as a convenient model. We examined the partition coefficient (log K_{LW}) between water and the dipalmitoyl L-α-phosphatidylcholine (DPPC) MLV for six thiophosphoryl OPs (P=S) and the corresponding oxons (P=O) at 25 and 60°C,[18] as shown in Fig. 1A. Since the phase transition temperature of DPPC is around 41°C, the MLV membrane shows the gel and more fluid liquid crystalline phases at 25 and 60°C, respectively. The linear correlation of log K_{LW} with log K_{ow} ($r^2=0.92$) was obtained for twelve OPs at 60°C, while the log K_{LW} *vs.* log K_{ow} plot showed the biphasic profile at 25°C with much less sensitivity of P=O against log K_{ow} than that of P=S. Furthermore, in order to examine the solubilized site of the OP in the MLV, we utilized fluorescence probes, 1,6-diphenyl-1,3,5-hexatriene (DPH) and its trimetylammonium derivative (tma-DPH). They are respectively dissolved in the hydrophobic core of alkyl chains and hy-

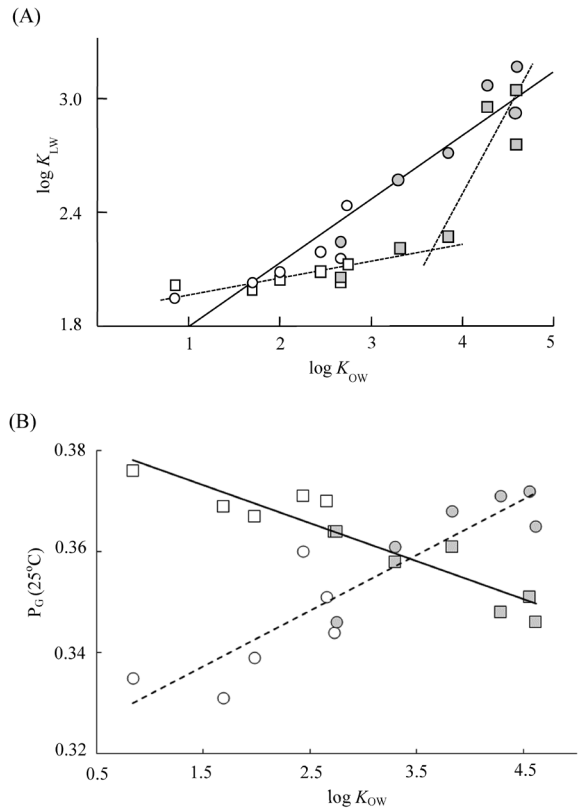

Fig. 1. Behavior of organophosphorus pesticides in the DPPC-MLV. (A) Partition coefficient (log K_{LW}) between water and the DPPC-MLV *vs.* log K_{ow}. Symbols indicate the pesticide having the P=S (gray) or P=O (open) moiety in the gel phase at 25°C (square) and the liquid crystalline one at 60°C (circle). (B) Fluorescence polarization (P_G) of probes *vs.* log K_{ow}. P_G was measured in the gel phase of the DPPC-MLV at 25°C. Symbols indicate the pesticide having the P=S (gray) or P=O (open) moiety in the presence of tma-DPH (circle) and DPH (square).

drophilic glycerol backbone/ester regions of a lipid bilayer, and their fluorescence polarization (P_G) decreases with an increase in membrane fluidity that is controlled by temperature and a co-solubilized molecule. The P_G value of DPH at 25°C proportionally decreased with the increasing log K_{ow} of the OP and that of tma-DPH showed the opposite profile (Fig. 1B), indicating that the incorporation of P=S and P=O into the DPPC-MLV increases the membrane fluidity in the neighborhood of DPH and tma-DPH, respectively. These results clearly show that P=S and P=O are located in the hydrophobic and hydrophilic regions of the DPPC bilayer, respectively, depending on their log K_{ow} in the gel phase. A similar approach with the additional fluorescence probe chlorophyll *a* was taken for the partition of phenoxyalkanoic acid herbicides to the MLV, and the undissociated 2,4-D was shown to reside in the hydrophilic region of DPPC bilayer.[19] This phenomenon was in good agreement with the uptake profiles of carboxylic acid metabolites of pesticides by duckweed (*Lemna gibba*).[20]

2. Hydrolysis

The hydrolysis mechanism is usually difficult to predict based on the product analysis alone. The approaches using a kinetic isotope effect and linear free energy relationship are very useful to investigate a reaction mechanism, but more time and effort are required to conduct a synthesis of many derivatives and their hydrolysis studies. Another approach is the quantum chemical method, which calculates the enthalpy change along a reaction coordinate and specifies the transition states (TSs) based on possible mechanisms.[21] We have applied this method to the alkaline hydrolysis of methyl and phenyl *N*-methylcarbamates[22] and phosphoryl and thiophosphoryl fluorides.[23] These studies showed that the hydration of a reactive species such as OH^- should be considered in calculations for the refined analysis.

We next examined the hydrolysis of herbicide flumioxazin (**I**) (Fig. 2), which undergoes base-catalyzed opening of the imide ring to the half amide (**II**), followed by acid-catalyzed cleavage of the amide bond of **II** to form **III**–**V**.[24] Since the amide bond of an amic acid is known to be cleaved *via* the intramolecular attack of an adjacent carboxyl group, the kinetic analysis was conducted according to the scheme in Fig. 2. The k_2 and k_{-1} rate constants could be well fitted by the equations $k_2=(k_W+k_H[H^+])/(1+K_a/[H^+])$ and $k_{-1}=(k'_W+k'_H[H^+]+k_O)/(1+K_a/[H^+])$, where k and k' are the rate constants, with the subscripts W, H, and O meaning neutral, acid-, and base-catalyzed hydrolysis, respectively. Almost the same dissociation constant (K_a) of **II** (4.38 and 4.41) was obtained by the regression analyses on k_2 and k_{-1}, indicating the carboxyl group as a key reactant.

In order to clarify the reaction mechanism, the AM1 MO calculations were conducted for the hydrolysis of *N*-methylmaleamic acid as a model of **II**.[25] The TS was searched using a reaction coordinate method, with its structure optimized by the NLLSQ routine, and it was confirmed by the presence of only one negative eigen vector in the FORCE calculation. As shown in Fig. 3, the intramolecular cyclization (S_0 to T_0) was examined using the atomic distance of C3–O6 as a reaction coordinate. The formation of a zwitterionic intermediate $S_\pm$ was highly endothermic (42.9 kcal mol^{-1}), but the hydration of water molecules to the amide and carboxyl oxygen atoms markedly reduced the enthalpy change to 2.1 kcal mol^{-1}. The cyclization thus proceeded *via* TS1 with an activation energy (E_a) of 7.4 kcal mol^{-1} under hydration. Next, when the C3–N4

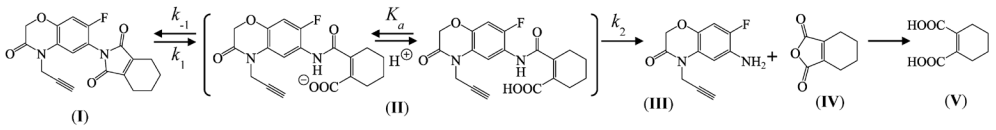

Fig. 2. Hydrolysis scheme of herbicide flumioxazin (**I**). k_1, k_{-1} and k_2 are the rate constants, and K_a is the dissociation constant.

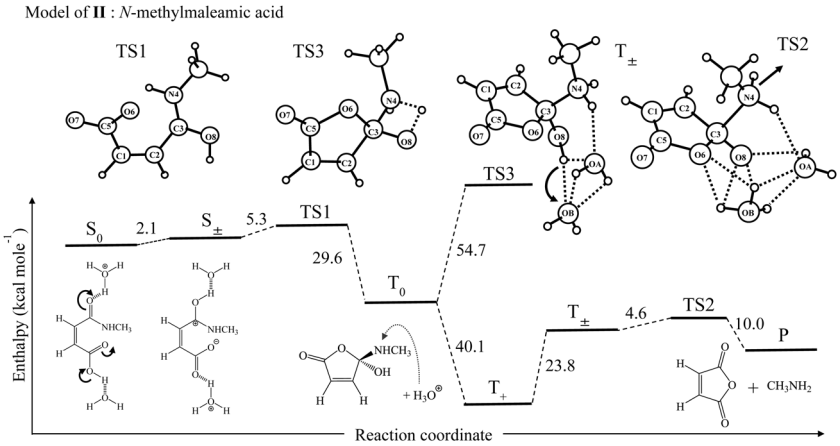

Fig. 3. Reaction coordinate analysis on hydrolysis of model *N*-methylmaleamic acid. TS and P indicate a transition state and products, respectively. OA and OB are oxygen atoms of water molecules. The dashed lines in the molecular structures mean hydrogen bonds.

atomic distance was taken as a reaction coordinate, the high E_a value of 54.7 kcal mol^{-1} was required for elimination of the methylamino moiety *via* TS3 where the proton concomitantly transferred from O8 to N4. In contrast, the intermediate $T_{\pm}$ was formed from T_+, the hydrated T_o with protonation at N4, with a lower enthalpy change of 23.8 kcal mol^{-1}. The E_a value of the following amine elimination from $T_{\pm}$ *via* TS2 was calculated to be 4.6 kcal mol^{-1}. As a result, the estimated E_a of 28.4 kcal mol^{-1} in total was very close to the experimental value. These analyses again show the importance of hydration in the quantum chemical calculations for hydrolysis.

3. Aqueous Photolysis

By absorbing sunlight at a wavelength >290 nm, a pesticide molecule is activated to excited states and undergoes chemical reactions, called direct photolysis.[7,26] Another degradation process is indirect photolysis, typically chemical reactions with photogenerated reactive species, such as hydroxyl radical (·OH) and singlet oxygen ($^1O_2$).[26] The usual photolysis experiments with a pesticide to examine its dissipation and transformation products do not directly give any information on reactive species, which is needed to scrutinize the photoreaction mechanism.

3.1. Photoinduced bond cleavage

Pyrethroid insecticide fenvalerate undergoes efficient photoinduced decarboxylation in water with the concomitant formation of many photoproducts.[27] The photolysis of twenty-five synthetic analogues of fenvalerate has shown that an α-substituent of the 3-phenoxybenzyl moiety primarily controls the yield of decarboxylation.[28] To investigate the mechanism of this reaction, we introduced a new photochemical index, ΔM_{ij} (A–B).[21,28] This index describes the change in electron density between two atoms (A and B) *via* one-electron transition from the *i*-th to *j*-th MO, which can be estimated by spectral simulation using the CNDO/S MO calculation with configuration interactions (CIs). The positive and negative signs of this index mean the possible formation and cleavage, respectively, of a bond between two atoms by excitation. When the α-substituent was hydrogen or an ethynyl group, the main transition was $n \rightarrow \pi^*$ with the large positive ΔM_{ij} value for the O–C (α-cyano-3-phenoxybenzyl) bond. In contrast, the cyano substitution changed the transition to $\pi \rightarrow \pi^*$ with the large negative ΔM_{ij} for this bond, clearly indicating the efficient photoinduced β-cleavage of fenvalerate prior to decarboxylation. Although the radical intermediates of fenvalerate trapped by the nitroso and *N*-oxide reagents had been detected by ESR,[29] we tried to catch them by applying another spin-trapping technique combined with a fluorescence probe, as shown in Fig. 4A.[30,31] The benzyl radical intermediate ($R\cdot$) was first trapped by the 3-amino-2,2,5,5-tetramethyl-

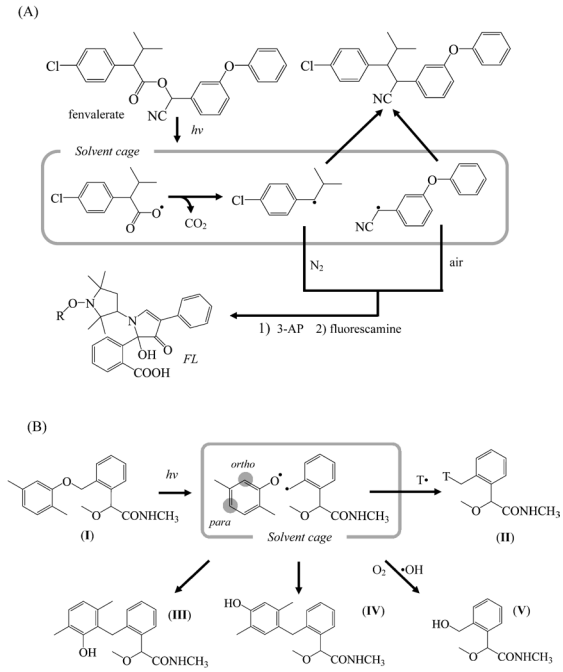

Fig. 4. Photodegradation of (A) insecticide fenvalerate and (B) fungicide mandestrobin (**I**). R is the benzyl radical formed from the acid or alcohol moiety of fenvalerate. T· is an *N*-oxide radical.

1-pyrrodinyloxy radical (3-AP), and the resultant adduct was derivatized with fluorescamine to the fluorescent product (*FL*). The photodegradation of [^{14}C] fenvalerate under air gave the adduct and *FL* of its α-cyano-3-phenoxybenzyl moiety, which were detected by HPLC with radio- and fluorescence detectors and identified by LC-MS. The corresponding adduct of the 4-chloro-α-isopropylbenzyl moiety was only detected under N_2 due to its higher reactivity against O_2.

We also succeeded in trapping one radical intermediate in the photo-Claisen rearrangement of the strobilurin fungicide mandestrobin (**I**) (Fig. 4B).[32] The addition of a radical trapping reagent (T·) produced the corresponding adduct (**II**) which was identified by LC-MS, clearly showing that the homolytic cleavage of the central O–C (benzyl) bond was a primary process, followed by the recombination of two radicals. The delocalization of an electron to the *ortho* and *para* positions against the phenoxy oxygen with the former position closer to the benzyl radical center resulted in more favorable formation of **III** than **IV**. Similar regioselectivity is observed for the photo-Fries rearrangement of *O*-aryl *N*-methylcarbamates.[33] Incidentally, aqueous photolysis of **I** showed greater formation of **V** in the presence of humic acid. The radical adduct of ·OH with 5,5-dimethyl-1-pyrroline *N*-oxide was formed in a dilute humic acid solution under irradiation, as detected by ESR. Therefore, ·OH generated by the photoexcited humic acid was most likely to react with the benzyl radical escaping from a solvent cage, leading to the formation of **V**.

3.2. Photoinduced bond formation

Azole fungicide diniconazole (**I**, X=Cl) rapidly undergoes geometrical isomerization under irradiation. The main photoproducts of **I** were *Z*-isomer (**II**) and its cyclized derivative (**III**), as shown in Fig. 5.[34] To investigate this reaction mechanism, the optimized molecular geometry of **II** (X=Cl) with θ_1=44° and θ_2=51° was first obtained *via* the AM1 MO calculations. In order to estimate its solution-phase molecular geometry, we obtained the spin-lattice relaxation times (T_1) of H_o and C1 in the phenyl ring (Fig. 5) by measuring the ^{1}H and ^{13}C NMR of **II** (X=Cl), which are related to the sum of the reciprocal of the distance from a neighboring atom to the sixth power. By comparing the observed T_1 (H_o) value with the calculated one which was derived from these atomic distances, both θ_1 and θ_2 were

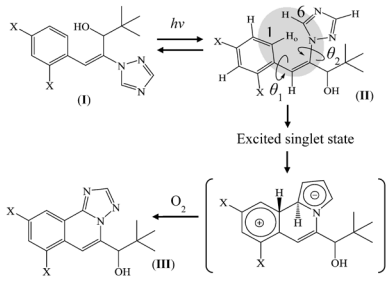

Fig. 5. Photodegradation of fungicide diniconazole (**I**; X=Cl). θ_1 and θ_2 are the torsional angles for the phenyl and 1,2,4-triazolyl rings.

Table 1. Photochemical reaction index for cyclization of **II** (X=F)

Absorption (nm)	Electronic transition	CI%[a]	ΔM_{ij} (C1–C6)[b]
258.3	HOMO→LUMO	58	+5.37
	HOMO→(N+1)LUMO	28	−5.60
285.4	HOMO→LUMO	59	+5.80
	HOMO→(N+1)LUMO	17	−5.60
287.3	HOMO→LUMO	30	+5.80
	HOMO→NLUMO	25	+5.37

[a] Percent of contribution in the configuration interaction. [b] Photochemical reaction index. HOMO, highest occupied MO; LUMO, lowest unoccupied MO; NLUMO and (N+1)LUMO, second and third lowest unoccupied MO, respectively.

estimated to be 28.9°. Since almost the same photochemical profiles of **II** were observed, irrespective of any halogen atom (X), and the atomic parameters of Cl were unavailable in CNDO/S, the spectral simulation was conducted for **II** (X=F). The estimated absorption wavelengths, as listed in Table 1, were close to the observed ones in methanol at 250 nm (ε=9680 $M^{-1}cm^{-1}$) and 286 nm (shoulder, ε=580 $M^{-1}cm^{-1}$). The photochemical index ΔM_{ij} (C1–C6) estimated for one-electron transition with the higher CI% mainly exhibited positive signs, strongly suggesting the photoinduced bond formation between C1 and C6, leading to the formation of **III**.

4. Chemical Reactions on Solid Surfaces

4.1. Photolysis on soil and plant

In the photodegradation (>290 nm) of pyrethroid insecticide [^{14}C] (1*R*)-*trans*-phenothrin (**I**) on the soil thin-layer, significant oxidative reactions at the isobutenyl side chain proceeded,[35] as shown in Fig. 6. Some of the main products were **II** and **III**, which should be formed *via* the ene reaction of **I** with $^1O_2$ (a), and others were **IV** and **V**, possibly formed *via* the cycloaddition of **I** with $^1O_2$ (b). Although **IV** and **V** can be also formed by the reaction with O_3 *via* ozonide (c), their formation even under the controlled flow of air passing through alkaline solution removing O_3 shows its minor contribution to this study. The aqueous solution of 2,2,6,6-tetramethyl-4-piperidone in the presence of humic substances extracted from the tested soil showed an ESR signal of the corresponding *N*-oxide radical by irradiation, and the coexistence of $^1O_2$ quencher NaN_3 significantly reduced this signal. Therefore, $^1O_2$ should be generated by energy transfer from the excited humic substances to molecular oxygen under irradiation. Similar degradates to **IV** and **V** were detected as main products on the leaf surface when the cabbage metabolism study of the insecticide [^{14}C] (1*R*)-*trans*-metofluthrin was conducted in the controlled greenhouse.[36] Four diastereomers of ozonide *via* reaction of the prop-1-enyl side chain with O_3 in air were detected by HPLC, and their structures and stereochemistry were confirmed by ^{13}C-, 1D/2D-^{1}H-NMR, and LC-MS. Incidentally, the photolysis of pesticides is one of the primary reactions on a plant surface, and a convenient model system would be useful instead of using intact plants. We ex-

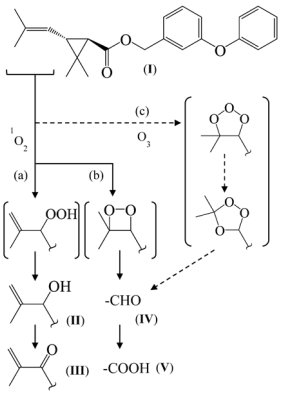

Fig. 6. Photodegradation of insecticide (1*R*)-*trans*-phenothin (**I**) on soil surface. (a) Ene reaction path; (b) cycloaddition path; (c) ozonide formation path.

amined the applicability of glass plates coated with plant waxes extracted from tomato fruits and leaves.[37] [Ph-^{14}C] fenitrothion applied to the wax-coated plates was transformed by irradiation at >290 nm to the corresponding oxon, *S*-isomer, and phenol in profiles similar to those observed in the intact plants. Therefore, this approach using appropriate plant waxes should be useful to examine the contribution of photolysis prior to the plant metabolism study of pesticides.

Next, we investigated the contribution of indirect photolysis at >300 nm for esfenvalerate, a (2*S*,α*S*)-isomer of fenvalerate, on thin films of Japanese upland soil and kaolinite.[38] The degradation half-life was extremely short (*ca.* 1 week) on kaolinite as compared to that on soil (around 3 months), with more formation of α-amide (**I**) and desphenyl (**II**) derivatives (Fig. 7). Direct photolysis was unlikely at >300 nm, since the reflectance spectrum of esfenvalerate on kaolinite was similar to its absorption one (λ_{max}=177 nm, ε_{300}=0). However, dark reaction of esfenvalerate with H_2O_2 in the presence of kaolinite formed **I**. The reaction of esfenvalerate with ·OH generated by Fenton's reagent formed **II**, and MS analysis showed that about 45% of ^{18}O was incorporated into **II** when the photodegradation was conducted on the kaolinite thin-layer prepared with $H_2{}^{18}O$. Similar photoinduced desphenylation was observed for 3-phenoxybenzoic acid (PB acid) on kaolinite.[39] Since we had suggested the formation of ·OH and H_2O_2 on photoirradiated kaolinite (Fig. 7) through photodegradation of the fungicide tolclofos-methyl,[40] the above results indicated that the photogenerated H_2O_2 and ·OH on kaolinite reacted with esfenvalerate in indirect photolysis to form **I** and **II**, respectively.

4.2. *Chemical reactions in/on soil*

Fenpropathrin is a pyrethroid insecticide with an α-cyano-3-phenoxybenzyl moiety, and the cyano group is transformed stepwise to α-amide and α-carboxyl ones in soil. We paid attention to the facts that they are minor products in soil metabolism under the water content kept at *ca.* 50% of a maximum water-holding capacity (MWHC),[41] and that the slower dissipation of fenpropathrin had been reported in the field by the soil mixing application of its formulation, as compared with its spray application to the soil surface.[42] Incidentally, the α-amide derivative was formed significantly (4–36%) on the soil thin-layer without controlling the soil water content in the photodegradation study, and the insignificant differences in its formation were observed between sunlight exposure and dark conditions,[43] showing that photolysis is of minor importance. When fenpropathrin was incubated in darkness by varying the water content of three Japanese upland soils from the oven- or air-dried condition to 10–100% of MWHC, the formation rate of the α-amide derivative increased markedly in the dried soils by a factor of 10–100 over the moistened ones, with no correlation of the soil organic matter content.[44] Its final yield was 67–84% in the air-died clay (kaolinite) prepared from the Ushiku soil, comparable to that in the air-dried soil. It is known that the surface acidity of kaolinite is a function of water content, and it corresponds to that of concentrated H_2SO_4 under the oven-dried condition.[7] Therefore, the observed transformation of the cyano group to a carboxyl one *via* the amide in fenpropathrin is most likely through acid-catalyzed hydration on a dried clay surface.

We next encountered the very unique nitration of the fungicide diethofencarb (**I**) at the 6 position of the phenyl ring in a moisture-controlled soil metabolism study (Fig. 8).[45] When **I** was incubated at 20°C and 50% MWHC for a week in fourteen Japanese upland soils, kaolinite and montmorillonite, the formation of the 6-NO_2 derivative (**II**) varied primarily with the percentage of clay and next with the percentage of organic matter and pH of the soil, as shown in Fig. 8.[46] The clay minerals, such as kaolinite, montmorillonite and allophane were obviously the most important factor, indicating that the nitration proceeded on the clay surface. Among the soils with a similar percentage

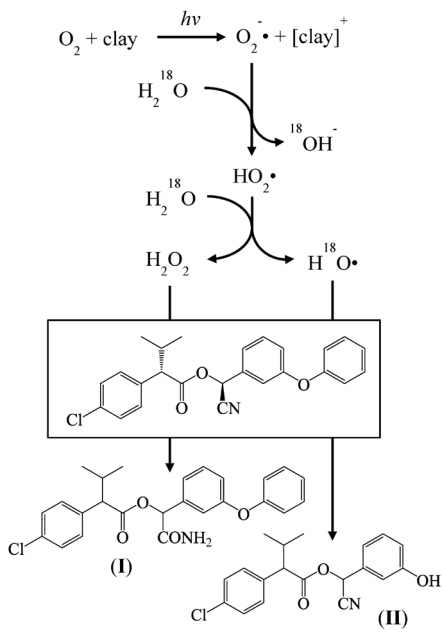

Fig. 7. Indirect photolysis of esfenvalerate by active oxygen species photo-generated on clay surface.

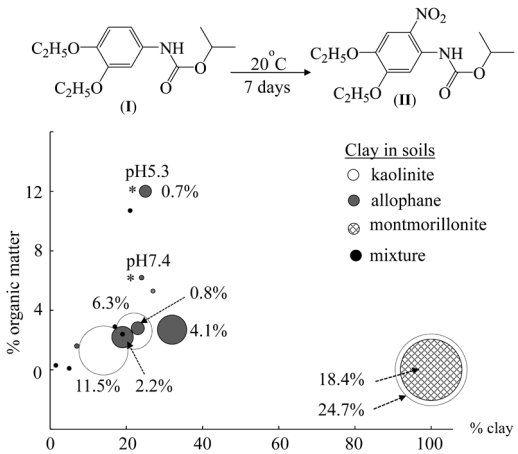

Fig. 8. Soil metabolism of diethofencarb (**I**) in soil. The bubble chart shows the percentage of 6-NO_2-diethofencarb (**II**) formation.

of clay, more **II** was formed in the lower-pH soil even if it contained a higher amount of organic matter (* in Fig. 8). In order to clarify the reaction mechanism, we measured the formation rate (k_n) of the 6-NO_2 derivative for five analogues of **I**, isopropyl 4-substituted phenylcarbamates, in the air-dried kaolinite. The linear free-energy relationship analysis showed a good relationship of log k_n with the Hammett σ^+ (slope, -7.75), indicating that the nitration of **I** is an electrophilic reaction. Since the dried clay surface exhibits high acidity, as described above, the nitration of **I** should be an acid-catalyzed reaction by a nitronium ion generated on the clay surface from intrinsic NO_3^-. The AM1 MO calculations for **I** showed that a much higher electron density in HOMO was located at the 6 position of the phenyl ring than at the 2 or 5 position, supporting this mechanism. Incidentally, the uptake of **II** from soil to plants was insignificant, and its mammalian toxicity was low without mutagenicity. Comparing its PEC with the ecotoxicity, **II** is unlikely to have any impact on the environment.

5. Water-Sediment System

5.1. *Effects of experimental conditions*

We examined the effect of aeration on the behavior of water-spiked [Ph-^{14}C] fenitrothion in the water-sediment systems at a water to sediment depth ratio of 6 : 2.5 (Fig. 9) in darkness, using samples collected from the French lake and Japanese pond.[47] An almost constant redox potential (E_h) was observed for water in a moderately oxidizing state by the bubbling of air *via* route (2), which changed the redox state of sediment from reducing to oxidizing. In contrast, the measurement of E_h showed that the simple airflow over water *via* route (1) caused a moderate reducing state of water but the reducing state of sediment was kept constant. Air bubbling *via* route (2) accelerated the mass transfer from water to sediment by agitation of the water, resulting in the shorter dissipation half-life (DT_{50}) of fenitrothion in water. Since the static overflow of air (1) made the system more reducing with time, more of the amino derivative of fenitrothion was formed, as compared with air bubbling (2).

Next, [Ph-^{14}C] fenitrothion was separately applied to water and sediment collected from the same Japanese pond under the overflow of air, each simulating the entry route of a spray drift and erosion, respectively.[48] The time-dependent ^{14}C distribution was monitored for overlying water, upper and lower sediment (0–0.5 and 0.5–2.5 cm depth), and pore water separated by centrifugation of the sediment. More ^{14}C exchange between water and the upper sediment was clearly observed here than between the sediment layers. The DT_{50} value of fenitrothion in the total system was almost insensitive to the application method, but with different degradation profiles between the application methods. The corresponding phenol, amino and its desmethyl derivatives were detected in the overlying water and the upper sediment, each of which amounted to *ca.* 10% in total with the water application, while the amounts of the former two were much lower with the sediment application, with the latter mainly present in the overlying water. These results may show that the resulting phenol is further degraded by sediment microbes, and the amino derivative is tightly bound to the sediment, as evidenced by the greater formation of bound ^{14}C in the sediment application, but more hydrophilic amino desmethyl derivative is released to the water.

5.2. *Effect of illumination*

In the natural environment, the overlying water is diurnally exposed to sunlight.[5] In order to examine the illumination effect on the pesticide behavior, we conducted water-sediment studies not only in darkness but also with exposure to simulated sunlight (Fig. 9) for several pesticides with different physicochemical properties and abiotic degradation profiles, as listed in Table 2. Plant growth regulator uniconazole-P (**I**) is resistant to hydrolysis, but it is rapidly photodegraded, similarly to diniconazole, to form the *Z*-isomer and cyclized compound. Illumination greatly accelerated its dissipation in the water-sediment system by a factor of *ca.* 80, which can be accounted for by the rapid photolysis of **I** in the overlying water, because of its slow partition to sediment due to moderate hydrophobicity.[49] The higher hydrophobicity of insect growth regulator pyriproxyfen (**II**) resulted in its faster partition from water to sediment, but

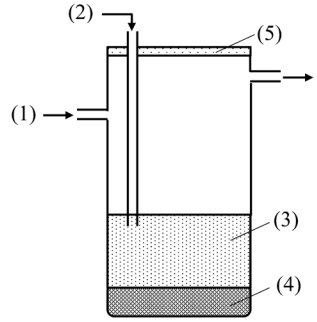

Fig. 9. Apparatus used in the water-sediment study. (1) Overflow of air, (2) air bubbling, (3) water phase, (4) sediment phase, (5) borosilicate glass cover (in darkness) or Pyrex glass filter (under irradiation by artificial sunlight).

Table 2. Effect of photolysis on pesticide profiles in water-sediment system

Factor	Uniconazole-P (**I**)	Pyriproxyfen (**II**)	Flumioxazin (**III**)	Esfenvalerate (**IV**)
log K_{ow}	3.67	5.37	2.6	6.2
DT_{50} [a)]				
hydrolysis	resistant	resistant	0.7 (pH 7)	428 (pH 7)
photolysis	0.5 (pure water)	4–6 (pH 7)	0.2 (pH 7)	2 (pH 7)
Water-sediment system				
Origin	U.K. pond	U.K. lake	U.K. lake	Japanese pond
Associated water				
DOC [b)]	8	7.8	—	—
pH	8.0	6.9	7.9	8.4
Sediment				
texture	loam sandy	clay loam	silt loam	sandy clay
% o.c. [c)]	6.8	3.4	4.9	2.7
pH	7.7	6.1	7.9	7.4
Conditions [d)]	Incubated at 20°C in darkness (D) or under irradiation (L)			
DT_{50} (L/D) [e)]	1.4/109.3	3/9	0.2/0.2	16/4.7

[a)] Dissipation half-life in a day. [b)] Dissolved organic carbon in mg carbon L^{-1}. [c)] Percent of organic carbon. [d)] Irradiation at 300–400 nm (6.7 MJ m^{-2} day^{-1}) for 8 hr day^{-1} for **I**, **III** and **IV**; at 300–800 nm (343 W m^{-2}) for 12 hr day^{-1} for **II**. [e)] For the water-sediment system in a day.

its moderate photoreactivity in water resulted in the threefold acceleration of dissipation by illumination.[50] When a pesticide is very susceptible to hydrolysis, the illumination effect should be masked. Herbicide flumioxazin (**III**) is rapidly hydrolyzed to its half-amide *via* opening of the imide ring, and both **III** and the half-amide should be slowly partitioned to sediment due to much less hydrophobicity. They are also rapidly photodegraded to azetidin-2-one derivatives likely *via* spiro and ketene intermediates.[51] Since the degradation half-lives of **III** in hydrolysis and photolysis at pH 7 are 0.7 and 0.2 days, respectively, the illumination effect in the water-sediment system was not observed. If a pesticide is rapidly partitioned from water to sediment due to its high hydrophobicity, photolysis in the overlying water cannot play a role in the water-sediment system. This is the case for the insecticide esfenvalerate (**IV**), which exhibits slow hydrolysis but rapid photolysis in water at pH 7, and no effect of illumination was observed.[52] These results indicate that the behavior in the water-sediment system should be most affected by illumination for hydrophilic or moderately hydrophobic pesticides resistant to hydrolysis but photolabile.

6. Oxidative Metabolism Model

Since the phase I oxidation catalyzed by the cytochrome P450 enzyme is most frequently a primary metabolic reaction, we investigated not only the applicability of the model system to estimate possible metabolites prior to *in vivo* metabolism study but also its reaction mechanism by using MO calculations.[21] The catalytic oxidation by P450 proceeds *via* the stepwise incorporation of two electrons and O_2 to finally form the oxo-iron (IV) porphyrin π-cation radical (OPCR), which transfers oxygen to a substrate molecule.[53] This reactive intermediate is known to be artificially produced *via* the so-called shunt pathway by the reaction with a peroxide. As a P450 model, we used several synthetic iron porphyrins with enough redox potential to oxidize a pesticide molecule (Fig. 10).[31,53] Fenvalerate underwent not only the cleavage of ester and ether linkages and hydration of the cyano group but also oxidation at the terminal phenyl ring at 2′ and 4′ positions to form 4′-OH and quinone (Q) derivatives,[53] as shown in Fig. 11, most of which were reported in plant and soil metabolism studies. In order to theoretically investigate the oxidation mechanism, we conducted MNDO-PM3 MO calculations to obtain the energy levels of several occupied MOs of esfenvalerate (2*S*, αS isomer),[53] and that of the $d\pi$–$p\pi$ MO ($E_{d\pi-p\pi}$) localized at each O-Fe^{IV}-Cl moiety of three OPCRs assuming the spin state of $S=3/2$ (quartet).[54] Incidentally, the perturbation theory qualitatively implies that the reaction proceeds efficiently between two sites where the energy levels of interacting MOs with high electron densities are close to each other. The energy diagram in Fig. 11 means the possible formation of 4′-OH, Q and desphenyl derivatives by the reaction with the OPCRs of Cl_8TPPFeCl and F_{20}TPPFeCl but not by that of $F_{20}Br_8$TPPFeCl, which is in good agreement with the experimental results.[53] Furthermore, we conducted oxidation of the insect growth regulator [^{14}C] pyriproxyfen by using F_{20}TPPFeCl and H_2O_2 in paral-

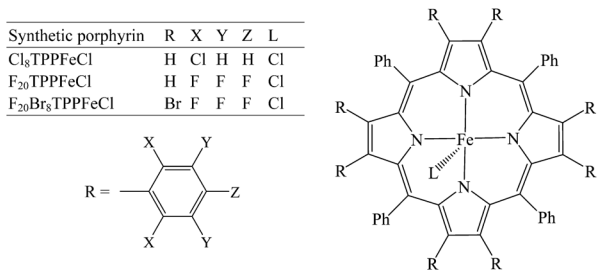

Fig. 10. Chemical structures of synthetic iron porphyrins as a P450 model.

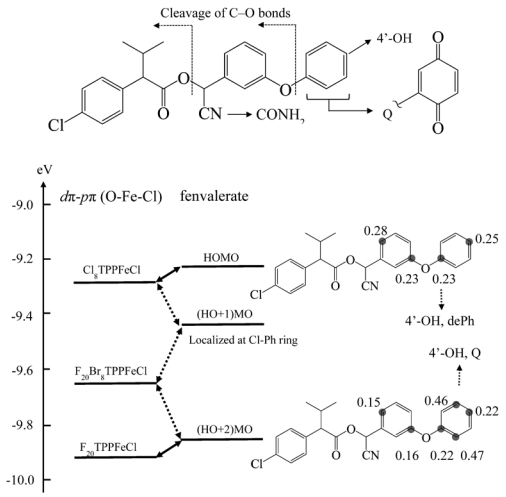

Fig. 11. Profiles of fenvalerate oxidation by iron porphyrins. Numbers around the chemical structures in the energy diagram are the electron density at the atom indicated by a filled circle for each MO.

lel with its *in vivo* metabolism in tomato fruits.[55] The porphyrin model reproduced almost all of the metabolites formed in tomato fruits, *via* the cleavage of an individual ether linkage and hydroxylation at the 4′ position of the phenoxyphenyl moiety.

Since the oxidative desulfuration of the thiophosphoryl OP pesticide to form oxon is known to be catalyzed by P450, we conducted our model reactions using three iron porphyrins and H_2O_2 to measure the oxidative dissipation rates (k) of four OPs, as listed in Table 3.[56] By assuming the same electrostatic interaction of the tested OPs with each OPCR from their structural similarities, the MO interaction between them was conveniently utilized to evaluate the oxidation. We estimated the $E_{d\pi-p\pi}$ values of OPCRs *via* regression analysis of the k values using the equation described in footnote e) of Table 3. The electronic parameters f_E and E_L of OPs with their geometries fully optimized were calculated *via* MNDO-PM3. These $E_{d\pi-p\pi}$ values are very close to those separately obtained using the same MO calculations of OPCRs ($S=3/2$), and this coincidence strongly supports OPCR as the key reactive intermediate in our oxidation model of P450, although some ambiguity remains due to the small data size in the regression.

We also investigated the reaction mechanism more in detail. *O*,*O*,*O*-Trimethyl phosphorothioate and oxene (biradical atomic oxygen) were used as simple models of OP and OPCR, respectively, in the reaction coordinate analysis for the singlet and triplet pathways (Fig. 12) using MNDO-PM3 MO calculations.[57] The two pathways were assumed: rearrangement *via* phosphoxathiirane (a) and abstraction–recombination *via* phosphine and sulfur monoxide (b). The formation of *S*-oxide was exothermic, irrespective of a spin state, from the enthalpy changes, −126.3 (singlet) and −98.4 (triplet) kcal mol^{-1}. Since less E_a in mechanism (a) was estimated for the triplet pathway (TS2, 12.0 kcal mol^{-1}) than the singlet one (TS1, 17.0 kcal mol^{-1}), mechanism (b) was further examined only for the triplet pathway. The triplet oxene abstracts sulfur from the *S*-oxide with E_a of 2.0 kcal mol^{-1} to form the intermediate adduct of phosphine and sulfur monoxide. The recombination to form the *O*-sulfide required a little more E_a (6.2 kcal mol^{-1}), indicating that mechanism (b) is more favorable than (a). The last step releasing sulfur from the *O*-sulfide was endothermic, with much less enthalpy change in the triplet pathway by *ca.* 50 kcal mol^{-1}. The reaction coordinate analysis showed the triplet abstraction–recombination mechanism most favorable in the gas phase. However, more investigation under a steric constraint in the neighborhood of the iron porphyrin moiety of P450 (OPCR) should be conducted.

Conclusion

We have been conducting a series of guideline studies and additional ones newly developed by ourselves to investigate the environmental behavior of pesticides. In order to clarify the reaction mechanisms of various transformation reactions, we have conducted not only a kinetic analysis based on organic chemistry using various chromatographic and spectroscopic methods but also a theoretical one using the MO calculations. We need to continuously investigate pesticide behavior with the accumulation of evidence, and at the same time, we need to develop new techniques to refine the environmental assessment of pesticides.

Table 3. Kinetic and quantum chemical analyses of porphyrin-catalyzed oxidation of organophophorus pesticides

Porphyrin		k[a]				$E_{d\pi-p\pi}$[d]
		Fenitrothion	Cyanophos	Tolclofos-methyl	Butamifos	
$F_{20}TPPFeCl$		0.061	0.298	0.123	0.169	−9.79[e]/−9.92[f]
$Cl_8TPPFeCl$		0.043	0.064	0.126	0.204	−9.26/−9.30
$Cl_8Br_8TPPFeCl$		0.052	0.040	0.030	0.014	−9.27/−9.64
HOMO	E_L[b]	−9.78	−9.56	−9.18	−9.57	
	f_E[c]	1.45	0.89	0.35	1.59	

[a] Dissipation rate constant (hr^{-1}) by porphyrin-catalyzed oxidation with H_2O_2 in $CHCl_3/CH_3OH$ (1 : 1, v/v) at r. temp. [b] Energy level (eV) of HOMO of pesticide localized at the thiophosphoryl sulfur atom. [c] Electrophilic reaction index at the thiophosphoryl sulfur atom. [d] Energy level (eV) of $d\pi$–$p\pi$ MO in the [O–Fe^{IV}–Cl] moiety of a model oxo-iron (IV) porphyrin π-cation radical (OPCR). [e] Estimated by the equation, $\log k = a + b * f_E / |E_L - E_{d\pi-p\pi}|$ (a, b: constant). [f] Calculated for each OPCR by MNDO-PM3, assuming the spin state of $S=3/2$.

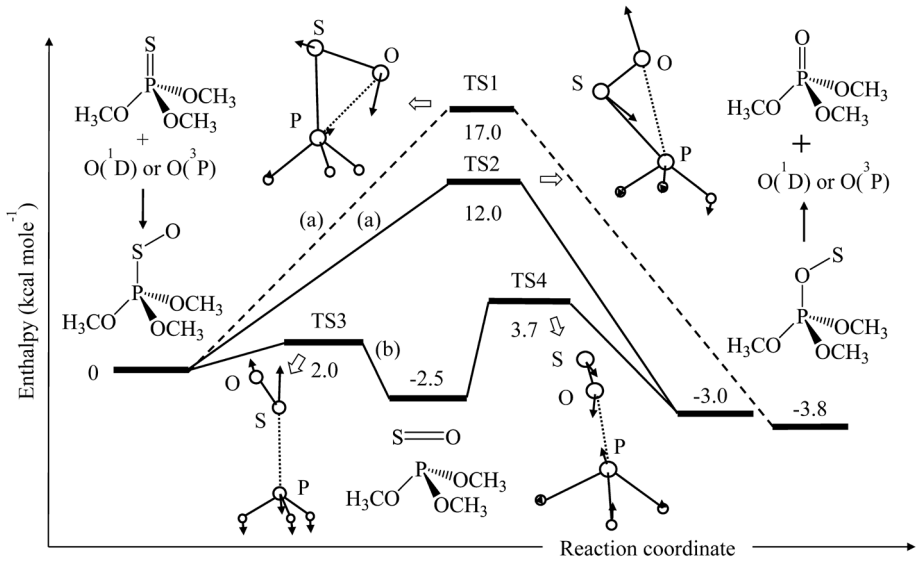

Fig. 12. Reaction coordinate analysis on the oxidative desulfuration of *O*,*O*,*O*-trimethyl phosphorothioate by oxene. O (^{1}D) and O (^{3}P) are the singlet and triplet oxene, respectively. TS means a transition state with arrows showing the vibrational mode of each atom. Dashed and solid lines indicate the singlet and triplet pathways for the rearrangement (a) and abstraction/recombination (b) mechanisms, respectively.

Acknowledgements

I feel honored that the Pesticide Science Society of Japan gave me an award. I am deeply grateful to Dr. Junshi Miyamoto (deceased), Dr. Hirohiko Yamada (deceased), Dr. Nobuyoshi Mikami, Dr. Yoshiyuki Takimoto, Dr. Masakazu Miyakado, Dr. Chiyozo Takayama, Dr. Takuo Fujisawa, all of the colleagues in the Environmental Health Science Laboratory and Agricultural Chemicals Research Laboratory of Sumitomo Chemical Co., Ltd., and Kyoto University professor emeritus Toshio Fujita (deceased).

References

1) T. Katagi: *Rev. Environ. Contam. Toxicol.* **175**, 79–261 (2002).
2) T. Katagi: *J. Pestic. Sci.* **38**, 10–26 (2013).
3) T. Katagi: *Rev. Environ. Contam. Toxicol.* **221**, 1–105 (2012).
4) T. Katagi: *Rev. Environ. Contam. Toxicol.* **187**, 133–251 (2006).
5) T. Katagi: *J. Pestic. Sci.* **41**, 121–132 (2016).
6) T. Katagi: *Rev. Environ. Contam. Toxicol.* **194**, 71–177 (2008).
7) T. Katagi: *Rev. Environ. Contam. Toxicol.* **182**, 1–195 (2004).
8) T. Katagi and N. Mikami: "Metabolism of Agrochemicals in Plants," ed. by T. R. Roberts, Chapt. 3, John Wiley & Sons, Ltd., New York, pp. 43–106, 2001.
9) T. Katagi: *Rev. Environ. Contam. Toxicol.* **204**, 1–131 (2010).
10) T. Katagi and H. Tanaka: *J. Pestic. Sci.* **41**, 25–37 (2016).
11) T. Katagi and K. Ose: *J. Pestic. Sci.* **39**, 55–68 (2014).
12) T. Katagi and K. Ose: *J. Pestic. Sci.* **40**, 69–81 (2015).
13) A. J. Leo: *Chem. Rev.* **93**, 1281–1306 (1993).
14) T. Katagi, M. Miyakado, C. Takayama and S. Tanaka: "Classical and Three-Dimensional QSAR in Agrochemistry," eds. by C. Hansch and T. Fujita, *ACS Symp. Ser*. 606, Chapt. 4, American Chemical Society, Washington D.C., pp. 48–61, 1995.
15) R. Wolfenden: *Science* **222**, 1087–1093 (1983).
16) S. E. Reynolds: *Pestic. Sci.* **20**, 131–146 (1987).
17) T. Katagi: *J. Pestic. Sci.* **26**, 165–168 (2001).
18) T. Katagi, M. Miyakado, C. Takayama and S. Tanaka: *J. Pestic. Sci.* **20**, 65–74 (1995).
19) T. Katagi: *J. Pestic. Sci.* **26**, 354–360 (2001).
20) T. Fujisawa, M. Kurosawa and T. Katagi: *J. Agric. Food Chem.* **54**, 6286–6293 (2006).
21) T. Katagi: "Rational Approaches to Structure, Activity, and Ecotoxicology of Agrochemicals," eds. by W. Draber and T. Fujita, CRC Press, Boca Raton, Chapt. 21, pp. 543–564, 1992.
22) T. Katagi: *J. Comput. Chem.* **11**, 524–530 (1990).
23) T. Katagi: *J. Mol. Struct. THEOCHEM* **538**, 157–164 (2001).
24) T. Katagi: *J. Pestic. Sci.* **28**, 44–50 (2003).
25) T. Katagi: *J. Comput. Chem.* **11**, 1094–1100 (1990).
26) T. Katagi: *J. Pestic. Sci.* **43**, 57–72 (2018).
27) N. Mikami, N. Takahashi, K. Hayashi and J. Miyamoto: *J. Pestic. Sci.* **5**, 225–236 (1980).
28) T. Katagi, N. Mikami, T. Matsuda and J. Miyamoto: *J. Chem. Soc., Perkin Trans. 2*, 779–782 (1989).
29) N. Mikami, N. Takahashi, H. Yamada and J. Miyamoto: *Pestic. Sci.* **16**, 101–112 (1985).
30) Y. Suzuki and T. Katagi: *J. Agric. Food Chem.* **56**, 10811–10816 (2008).
31) T. Katagi: "Pyrethroids From Chrysanthemum to Modern Industrial Insecticide," eds. by N. Matsuo and T. Mori, Springer, New York, *Top. Curr. Chem.* 314, Chapt. 8, pp. 167–202, 2012.
32) T. Adachi, Y. Suzuki, M. Nishiyama, R. Kodaka, T. Fujisawa and T. Katagi: *J. Agric. Food Chem.* **66**, 8514–8521 (2018).
33) T. Katagi: *J. Pestic. Sci.* **16**, 57–62 (1991).
34) T. Katagi: *J. Pestic. Sci.* **27**, 111–117 (2002).
35) Y. Suzuki, A. Lopez, M. Ponte, T. Fujisawa, L. O. Ruzo and T. Katagi: *J. Agric. Food Chem.* **59**, 10182–10190 (2011).
36) D. Ando, M. Fukushima, T. Fujisawa and T. Katagi: *J. Agric. Food Chem.* **60**, 2607–2616 (2012).
37) M. Fukushima and T. Katagi: *J. Agric. Food Chem.* **54**, 474–479 (2006).
38) T. Katagi: *J. Agric. Food Chem.* **39**, 1351–1356 (1991).
39) T. Katagi: *J. Agric. Food Chem.* **40**, 1269–1274 (1992).
40) T. Katagi: *J. Agric. Food Chem.* **38**, 1595–1600 (1990).
41) S. Sakata, J. Yoshimura, K. Nambu, N. Mikami and H. Yamada: *J.*

Pestic. Sci. **15**, 363–373 (1990).
42) R. A. Chapman and C. R. Harris: *J. Environ. Sci. Health* **16B**, 605–615 (1981).
43) N. Takahashi, N. Mikami, H. Yamada and J. Miyamoto: *Pestic. Sci.* **16**, 119–131 (1985).
44) T. Katagi: *J. Pestic. Sci.* **18**, 333–341 (1993).
45) S. Sakata, T. Katagi, J. Yoshimura, N. Mikami and H. Yamada: *J. Pestic. Sci.* **17**, 221–230 (1992).
46) R. Kodaka, T. Sugano, T. Katagi and Y. Takimoto: *J. Agric. Food Chem.* **51**, 7730–7737 (2003).
47) R. Kodaka, T. Sugano, T. Katagi and Y. Takimoto: *J. Pestic. Sci.* **27**, 235–241 (2002).
48) R. Kodaka, T. Sugano, T. Katagi and Y. Takimoto: *J. Pestic. Sci.* **28**, 175–182 (2002).
49) R. Kodaka, T. Sugano and T. Katagi: *Environ. Toxicol. Chem.* **25**, 310–316 (2006).
50) R. Kodaka, S. E. Swales, C. Lewis and T. Katagi: *J. Pestic. Sci.* **36**, 33–40 (2011).
51) A. Shibata, R. Kodaka, T. Fujisawa and T. Katagi: *J. Agric. Food Chem.* **59**, 11186–11195 (2011).
52) R. Kodaka, T. Sugano and T. Katagi: *J. Pestic. Sci.* **34**, 27–36 (2009).
53) M. Fukushima and T. Katagi: *J. Pestic. Sci.* **34**, 241–252 (2009).
54) T. Katagi: *J. Mol. Struct. THEOCHEM* **728**, 49–56 (2005).
55) M. Fukushima, T. Fujisawa and T. Katagi: *J. Agric. Food Chem.* **53**, 5353–5358 (2005).
56) T. Fujisawa and T. Katagi: *J. Pestic. Sci.* **30**, 103–110 (2005).
57) T. Katagi: *J. Comput. Chem.* **14**, 1250–1257 (1993).